Neuron
Article

Synchronized Network Oscillations in Rat Tuberoinfundibular Dopamine Neurons: Switch to Tonic Discharge by Thyrotropin-Releasing Hormone

David J. Lyons,[1,*] Emilia Horjales-Araujo,[1] and Christian Broberger[1,*]
[1]Department of Neuroscience, Karolinska Institutet, 171 77 Stockholm, Sweden
*Correspondence: david.lyons@ki.se (D.J.L.), christian.broberger@ki.se (C.B.)
DOI 10.1016/j.neuron.2009.12.024

SUMMARY

The pituitary hormone, prolactin, triggers lactation in nursing mothers. Under nonlactating conditions, prolactin secretion is suppressed by powerful inhibition from hypothalamic tuberoinfundibular dopamine (TIDA) neurons. Although firing pattern has been suggested as integral to neuroendocrine control, the electrical behavior of TIDA cells remains unknown. We demonstrate that rat TIDA neurons discharge rhythmically in a robust 0.05 Hz oscillation. The oscillation is phase locked between neurons, and while it persists during chemical synaptic transmission blockade, it is abolished by gap junction antagonists. Thyrotropin-releasing hormone (TRH) potently stimulates prolactin release, an effect assumed to take place in the pituitary. In TIDA cells, TRH caused a transition from phasic to tonic firing through combined pre- and postsynaptic effects. These findings suggest a model for prolactin regulation where a TIDA network switch from oscillations to sustained discharge converts dopamine from an antagonist at high concentrations to a functional agonist as dopamine output from the network decreases.

INTRODUCTION

The pituitary hormone, prolactin, initiates breast milk production post partum and exerts potent inhibition of fertility and sexual arousal (see Freeman et al., 2000). Unique among cells in the pituitary, prolactin-producing lactotrophs are controlled by hypothalamic inhibition rather than stimulation. The inhibitory signal is provided by neuroendocrine parvocellular tuberoinfundibular dopamine (TIDA) neurons in the arcuate nucleus (Arc) (Fuxe, 1964; "A12" population) that release DA into the portal capillaries of the median eminence for transport to the pituitary (Hökfelt, 1967; Björklund et al., 1973; see Ben-Jonathan and Hnasko, 2001). This powerful suppression explains why, despite a fully functional prolactin secretory system, lactation occurs only during nursing in women and in men not at all. The importance of tonic inhibition of prolactin release is illustrated by the potency of DA agonists in the treatment of prolactinoma, the most common form of pituitary tumor (Burrow et al., 1981), and by the hyperprolactinaemia and sometimes galactorrhea that is a side effect of antipsychotic drugs with DA antagonist properties (Clemens et al., 1974; Meltzer and Fang, 1976). Yet, to date, the cellular and network electrophysiological properties of the TIDA cell population have not been described. These factors are potentially fundamental features of prolactin regulation since discharge pattern may determine the functional output of neuroendocrine control of the anterior pituitary, as is observed in the magnocellular system (Wakerley and Lincoln, 1973; Hatton et al., 1983). Thus, the periodic bursting pattern in hypothalamic gonadotropin-releasing hormone neurons is required for stimulation of target gonadotrophs in the pituitary (Knobil, 1980). When bursting is artificially replaced by continuous agonist stimulation, gonadotropic hormone secretion is abolished (Nakai et al., 1978), a phenomenon that is exploited in treating, for example, gynecologic cancer and endometriosis.

To better understand the regulation of prolactin secretion, we have performed the first recordings from identified TIDA neurons. In addition, we have studied the effects of thyrotropin-releasing hormone (TRH) on this neuronal population. While no unique releasing factor has been assigned for lactotrophs, TRH, in addition to its role as master hormone of the thyrotropic axis, can potently stimulate prolactin secretion (Bowers et al., 1971; Jacobs et al., 1971; see Samson et al., 2003). These effects have been assumed to take place at the lactotroph itself. Here, we explored the novel possibility that TRH can act at the hypothalamic level to modulate the functional output of TIDA neurons. Our results show a robust 0.05 Hz oscillation of TIDA neurons that transforms to tonic firing in the presence of TRH, suggesting a mechanism for neuroendocrine inhibition. Part of the results have been previously presented in abstract form (D.J.L. et al., 2009, Soc. Neurosci., abstract).

RESULTS

TIDA Neurons Exhibit Robust, Rhythmic Oscillations

Whole-cell recordings where performed in rat Arc coronal slices. A highly stereotyped oscillation could be observed in a subpopulation of neurons (Figure 1Aa). This rhythmicity was characterized by periods of hyperpolarization and quiescence (DOWN states) alternating with periods of pronounced depolarization and action potential firing (UP states). The transition from UP to DOWN state was exceptionally regular, occurring at a

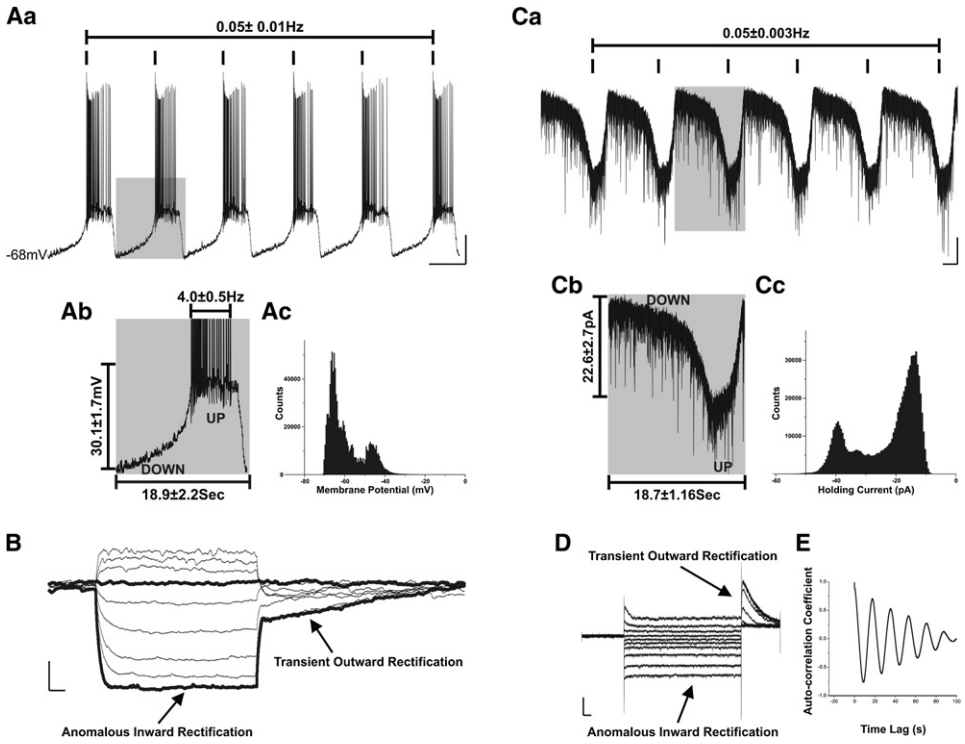

Figure 1. A Subpopulation of Arc Neurons Display Rhythmic Oscillations

(Aa) Current-clamp recording of a spontaneously oscillating neuron in the dorsomedial Arc (frequency 0.05 ± 0.01 Hz). Gray box in (Aa) expanded in (Ab) illustrates transition from hyperpolarized DOWN to depolarized UP state. Mean peak-to-trough amplitude (30.1 ± 7 mV) was calculated from the nadir of DOWN state to firing threshold of first action potential. Period (18.9 ± 2.2 s) was calculated from nadir to nadir. Mean UP state discharge frequency was 4.0 ± 0.5 Hz (n = five sequential UP states/cell in five cells). (Ac) Frequency plot highlighting the biphasic membrane voltage distribution of the oscillation depicted in (Aa).

(B) Superimposed membrane potential responses of an oscillating neuron to a series of increasing current steps of constant increment (range +18 to −45 pA). This was performed in the presence of TTX to abolish both action potential firing and oscillation. The resulting current-voltage relationship revealed the presence of characteristic voltage-dependent conductances; anomalous inward rectification and an A-like conductance (transient outward rectification).

(Ca) Voltage-clamp recording of a spontaneously oscillating neuron at a holding potential of −60 mV. Gray box in (Ca) is expanded in (Cb) and illustrates the periodicity and size of the current required to drive the cell through the oscillatory cycle (n = five sequential UP states/cell in five cells). (Cc) Frequency plot highlighting the biphasic current distribution of the oscillation depicted in (Ca).

(D) Superimposed membrane current responses of an oscillating neuron to a series of increasing voltage command steps of constant increment (range −120 to −30 mV), prepulse command potential −60 mV, postpulse command potential −40 mV. Voltage-clamp recording performed in the presence of TTX to abolish action potential firing and oscillation. Note characteristic voltage-dependent conductances; anomalous inward rectification and an A-like conductance (transient outward rectification).

(E) Autocorrelogram of the neuron depicted in (Aa) demonstrating strong autocorrelation with prominent side peaks indicative of 0.05 Hz rhythmicity.

Scale bar in (Aa) indicates 15 mV and 10 s, in (B) 20 mV and 0.2 s, in (Ca) 10 pA and 5 s and in (D) 50 pA and 0.2 s.

frequency of 0.05 ± 0.01 Hz (n = 5) with a peak-to-trough amplitude of 30.1 ± 1.7 mV (n = 5; Figure 1Ab). During UP states, an average of 19.8 ± 2.6 (n = 5) action potentials were discharged at a frequency of 4.0 ± 0.5 Hz (n = 5). Membrane potential distribution showed two distinct peaks across the oscillatory cycle, underscoring the biphasic nature of these Arc neurons (Figure 1Ac). The current-voltage relationship of oscillator neurons revealed two characteristic conductances: anomalous inward rectification (Katz, 1949) and a large A-like transient outward rectification (Connor and Stevens, 1971; Figures 1B and 1D). There was, however, no evidence of a depolarizing sag, indicative of the hyperpolarization-activated mixed cation conductance, I_h, commonly implicated in pacemaker rhythms (Lüthi and McCormick, 1998). When recorded in voltage clamp (holding potential −60 mV), Arc oscillator neurons exhibited similar temporal properties to those observed in current clamp, with alternating UP and DOWN states (Figure 1Ca). The transition from DOWN to UP required an inward current of 22.6 ± 2.7 pA (Figure 1Cb; n = 10). Plotting the injected current required during an oscillatory cycle mirrored the bimodal frequency distribution described above for membrane potential in current-clamp mode (Figure 1Cc). Correlation analysis (Figure 1E) revealed that the oscillatory behavior was highly regular, displaying powerful autocorrelation (n = 7/7).

Oscillator neurons represented only a small proportion of the total Arc neurons sampled (60/401; 15%) and were only encountered in the dorsal aspect of the Arc directly apposed to the third ventricle (Figure 2Aa). A portion of recorded cells were recovered for morphological reconstruction following dye filling. Neurons exhibiting the oscillation were typically of 20–30 μm diameter and extended four to five primary dendrites (Figure 2Ab). Nonoscillator neurons were encountered throughout the Arc and

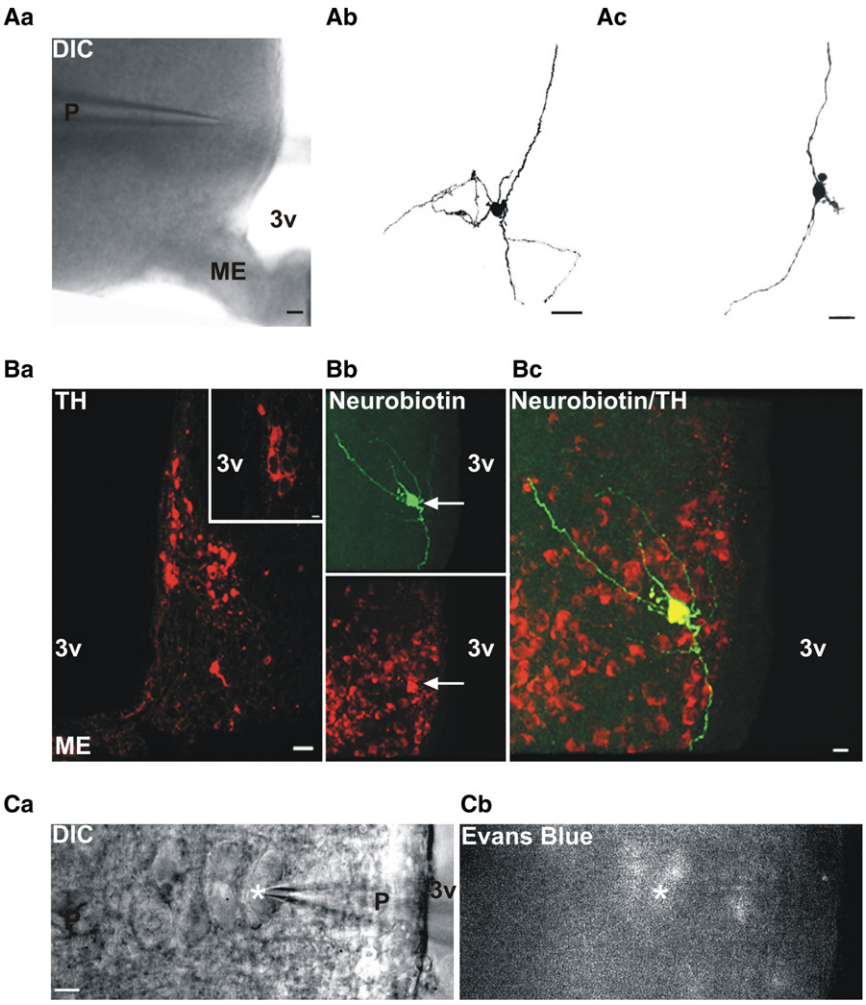

Figure 2. Oscillator Neurons Are Tyrosine-Hydroxylase-Positive Neuroendocrine Tuberoinfundibular Dopamine Neurons

(Aa) Differential interference contrast (DIC) micrograph of Arc slice during recording of an oscillator neuron. The tip of the recording pipette (P) is located in the dorsomedial (dm) Arc, adjacent to the third ventricle (3v). (Ab–Ac) A reconstructed oscillator neuron (Ab) with extensive dendritic arborization is shown next to a nonoscillator Arc cell (Ac) with largely unbranched dendrites.

(Ba) Confocal micrograph from coronal 14 μm thick section of the rat hypothalamus labeled with immunofluorescence for TH. Immunoreactive (ir) cells are seen primarily in the dorsal aspect of the Arc ("TIDA cells") with occasional additional TH-ir cells scattered in the ventromedial portion. Inset shows TH-ir cell bodies clustered closely together in the dmArc. (Bb and Bc) Confocal micrographs where a biocytin-filled recorded oscillator neuron (arrow) in a 275 μm thick slice preparation has been processed with avidin fluorescence (Bb; green) and stained with immunofluorescence for TH (Bc; red). Images in (Bb) shown merged in (Bc). The oscillator neuron is TH positive and extends dendritic arborizations throughout the field of TH-ir cell bodies.

(Ca) DIC image of an oscillator neuron (asterisk) from an animal injected i.v. with Evans Blue. The neuroendocrine nature of the cell is shown by its uptake of the fluorescent dye (Cb).

Scale bars indicate 50 μm in (Aa), 20 μm in (Ab)–(Ac), 50 μm in (Ba), 10 μm in (Ba) (inset), 20 μm in (Bc), 10 μm in (Ca). ME, median eminence.

though not of uniform morphology (as expected given the heterogeneity of this nucleus [Everitt et al., 1986]), in general exhibited distinctly less arborization, often with two sparsely branched primary dendrites extending from a bipolar soma (Figure 2Ac). In light of the discrete localization of oscillator neurons to the dorsal Arc, we explored the possibility that oscillator cells included the TIDA population. Sections of rat Arc were stained by immunofluorescence for the rate-limiting enzyme in catecholamine biosynthesis, tyrosine hydroxylase (TH), a marker for TIDA cells (Chan-Palay et al., 1984; van den Pol et al., 1984; Everitt et al., 1986). This staining revealed TH-immunoreactive (-ir) cells ("A12 population"; Fuxe, 1964) clustered closely together in the dorsomedial Arc, the location of the TIDA population (Figure 2Ba). From this cluster, TH-ir cells extended in a diagonal band toward the ventrolateral portion of the Arc, as previously described (Fuxe, 1964; Chan-Palay et al., 1984; van den Pol et al., 1984; Figure 2Ba). Immunofluorescence was then applied to dye-filled cells in slices used for electrophysiological recording. This staining revealed that all recovered oscillator cells (n = 11/11) were TH-ir (Figures 2Ba–2Bc). In contrast, out of ten recovered nonoscillator Arc cells, none stained positive for TH. Recovered TIDA cells could be seen extending their dendritic arborizations throughout the area occupied by TH-ir cell bodies (Figure 2Bc). To further evaluate the neuroendocrine nature of oscillator neurons, rats were injected with the blood-brain barrier impermeable dye Evans Blue, whose uptake can be used to identify neuroendocrine neurons (Weiss and Cobbett, 1992). Evans Blue fluorescence was observed in a significant minority of cells. In the Arc, seven oscillator cells recorded in hypothalamic slices from dye-injected rats were consistently (100%) Evans Blue positive (Figures 2Ca–2Cb). Taken together, location, morphology, neurochemistry, and neuroendocrine phenotype provide strong evidence that oscillator cells are indeed TIDA neurons.

TIDA Oscillations Are Synchronous and Gap Junction Dependent

Next, we sought to determine if the oscillations are network phenomena and, if so, which cell communication mechanisms underlie its propagation. Synaptic input was examined across UP and DOWN states. A significant increase in the frequency of inhibitory postsynaptic currents (IPSCs) was observed in UP (inter-event-interval (IEI) 188.4 ± 14.9 ms) as compared to DOWN (IEI 268.9 ± 7.8 ms; n = 3; $p < 0.05$; Figures 3Aa and

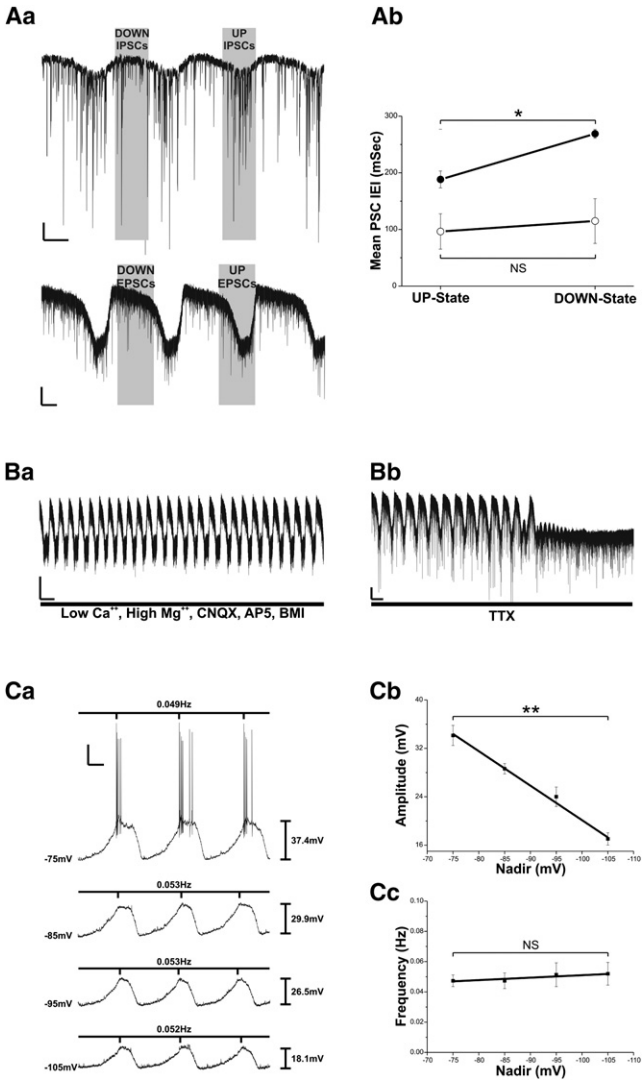

Figure 3. Network Properties of Oscillating TIDA Neurons

(Aa) Variation in synaptic intensity across UP and DOWN states. The top trace was recorded with "high Cl^-" pipette solution and in the presence of CNQX/AP5 to isolate IPSCs; the bottom trace was recorded in the presence of BMI to isolate EPSCs. Note the significantly increased incidence of IPSCs (●) during the UP state and uniform distribution of EPSCs (○) across UP and DOWN states (Ab) (n = 3; *p < 0.05).

(Ba) The oscillation endures in "low Ca^{2+}/high Mg^{2+}" and in the presence of blockers of fast synaptic transmission (n = 3/3). (Bb) The oscillation is abolished in the presence of TTX (n = 17/18).

(Ca) Current-clamp recording depicting the effect of progressive hyperpolarization upon oscillation dynamics. Note the diminished magnitude (Cb) and constant rhythmicity (Cc) (n = 3; **p < 0.01).

Scale bar in (Aa) (top trace) indicates 25 pA and 8 s, in (Aa) (bottom trace) 10 pA and 5 s, in (Ba) 10 pA and 30 s, in (Bb) 10 pA and 20 s, and in (Ca) 20 mV and 5 s. Error bars represent the mean ± SEM.

3Ab). No such difference was found for excitatory PSCs [EPSCs; IEI(UP) 96.4 ± 31.2 ms versus IEI(DOWN) 114.8 ± 39.5 ms; n = 3; Figures 3Aa and 3Ab]. Given the GABAergic nature of TIDA neurons (Everitt et al., 1984), these findings indicate the possibility of synaptic communication within the TIDA network. Surprisingly, however, the rhythmicity remained with unaltered temporal properties when ionotropic glutamate and GABA transmission were blocked through pharmacological antagonism (CNQX, AP5; BMI) or inhibition of Ca^{2+}-dependent synaptic transmission by recording in "low Ca^{2+}/high Mg^{2+}" solution (n = 3/3; Figure 3Ba). These results suggest that TIDA oscillations do not require synaptic communication. The application of the Na^+ channel antagonist, TTX, however, abolished oscillatory activity in all recorded cells except one where amplitude was diminished (n = 17/18; Figure 3Bb), indicating that rhythmic activity may depend on a TTX-sensitive conductance.

One possible interpretation of the above findings is that TIDA cells are autonomous pacemakers. When the oscillation was recorded under successive hyperpolarization (through the injection of negative holding current; Llinás and Yarom, 1986; Chorev et al., 2007; Tazerart et al., 2008), however, we observed that although UP state amplitude gradually decreased, oscillation frequency remained unaffected (n = 3; Figures 3Ca–3Cc; projected reversal potential −143 mV). This finding combined with the clustering of IPSCs during UP states suggests that rhythmicity may be propagated electrotonically from other, phase-locked, TIDA neurons. To determine the extent of oscillation synchrony across the TIDA population, we performed dual whole-cell recordings. Pairs of oscillator neurons recorded simultaneously demonstrated a high degree of synchronicity, with membrane potential fluctuations displaying marked fidelity across cells, extending even to individual UP state waveforms (n = 8/8; Figures 4Aa, 4Ab, and 4Ad). Cross-correlation analysis of simultaneously recorded neurons produced a Pearson correlation coefficient of 0.77 ± 0.08 (n = 8; Figure 4Ac). While our preceding experiments suggested that conventional, chemical, synapses are not required for TIDA oscillations, an alternative route for the network propagation of rhythmicity are gap junctions. Following prolonged application of the gap junction blocker carbenoxolone (Davidson et al., 1986; CBX; 50 μM; n = 5), the TIDA oscillation gradually weakened (evidenced as a successive loss of spectral density at the frequency of the oscillation; Figure 4Bd). Eventually a complete abolishment of autocorrelation (autocorrelation coefficient measured at apex of first side peak; control 0.70 ± 0.04; gap junction blockade 0.04 ± 0.01; n = 4; p < 0.005; Figure 4Bc) was observed. A similar effect was also seen in the presence of another uncoupling agent, 18β-glycyrrhetinic acid (Davidson et al., 1986; 18βGA; 50 μM; n = 7; Figure 4Ba, inset). We conclude that oscillations are synchronized throughout the TIDA cell network through gap junction-dependent mechanisms.

Thyrotropin-Releasing Hormone Replaces TIDA Oscillations with Tonic Firing

Thyrotropin-releasing hormone (TRH) is the most potent prolactin-releasing factor identified to date (see Samson et al., 2003). To explore the anatomical relationship between TRH and TIDA cells, sections of the Arc were processed for immunofluorescence double staining (Figures 5Aa–5Af). A dense network of TRH-ir terminals could be observed in the Arc (Figure 5Aa), with particularly high density in the dorsal aspect, where TH-ir cells were located (Figure 5Ab). Tyrosine hydroxylase-ir cell somata were surrounded by TRH-ir terminals (Figures 5Ac–5Af)

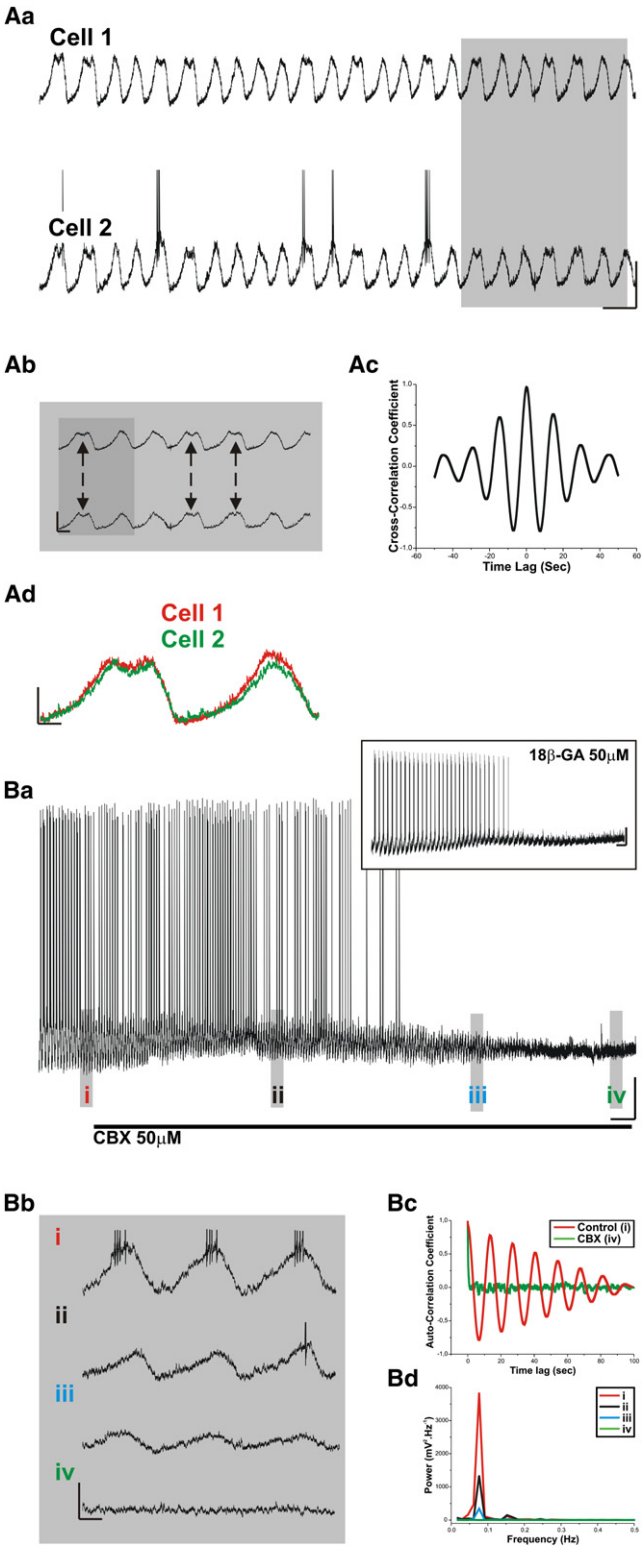

Figure 4. TIDA Oscillations Are Phase Locked and Abolished by Gap Junction Blockade

(Aa) Simultaneous subthreshold current-clamp recording of two TIDA neurons depicting a high degree of synchronicity (action potentials truncated for purposes of clarity). Gray box in (Aa) expanded in (Ab) highlights the strength of phase locking as even small deviations in UP state waveform are present in both cells (arrows). (Ac) Cross-correlogram of signals in (Ab) shows that TIDA neurons are powerfully cross-correlated with prominent side peaks indicative of 0.05 Hz rhythmicity. (Ad) Superimposition of UP states highlighted in (Ab). (Ba) Current-clamp recording depicting the abolishment of the TIDA oscillation following prolonged application of gap junction blockers CBX and 18β-GA (inset) (n = 12). Gray boxes in (Ba) expanded in (Bb) illustrate the gradual nature of this reduction. (Bc) Autocorrelogram of the data in (Ba, i) and (Ba, iv), note presence and absence of correlation in (i) and (iv) respectively. (Bd) Spectral analysis of the data in (Bb); note the progressive reduction in spectral density at the frequency of the oscillation.

Scale bar in (Aa) 20 mV and 20 s, in (Ab) 20 mV and 5 s, in (Ad) 10 mV and 2.5 s, in (Ba) 20 mV and 2 min, in (Ba) (inset) 20 mV and 20 s, and in (Bb) 20 mV and 5 s.

and, in higher magnification, numerous close appositions could be seen decorating the membrane of TH-ir cells, making contact both onto the cell soma and proximal dendrites (Figures 5Ae and 5Af). A few (one to two per section) TRH-ir cell bodies were observed within the dorsal Arc. These cells, however, were distinct from the TH-ir population (Figure 5Ad).

Our histochemical findings indicate the possibility of synaptic contacts between afferent TRH terminals and TIDA neurons. We were therefore interested to investigate if the prolactin-releasing effects of TRH could be underpinned by direct actions of the peptide on TIDA neurons. Application of TRH (1 μM) to oscillating Arc neurons consistently (n = 33/33; 100%) resulted in a depolarization and transition from phasic to tonic discharge (Figure 5Ba). This effect was evident in the frequency histogram as a shift from bi- to monophasic distribution (Figure 5Bb). The TRH-associated depolarization reversed and phasic firing was restored upon washout (Figure 5Ba). Action potential frequency was significantly slower during the TRH-induced tonic discharge (1.4 ± 0.4 Hz; measured at steady state; n = 4) than under control conditions in the UP state (4.2 ± 0.5 Hz; n = 5 sequential UP states/cell in 4 cells; $p < 0.05$). In the presence of TTX, TRH (1 μM) induced a significant mean depolarization of 13.1 ± 3.4 mV (n = 4/4; $p < 0.05$; Figures 6Aa–6Ac), indicating a direct postsynaptic effect that was also dose dependent (EC_{50} = 40.4 nM; n = 4; Figure 6Ab). Depolarization was not associated with a statistically significant change in input resistance (n = 4; Figure 6Ad). When fast synaptic transmission was blocked by the continuous application of CNQX, AP5, and BMI, the TRH-induced depolarization was still observed (+20.9 ± 1.3 mV; n = 6; $p < 0.005$; Figure S1), and action potential discharge switched reversibly from phasic to tonic, suggesting that this postsynaptic effect alone was sufficient to alter firing pattern in TIDA neurons. Responsiveness to TRH (1 μM) was observed also in nonoscillating neurons in the Arc encountered while sampling for TIDA cells. Though application of TRH (1 μM) elicited depolarization also in a portion of nonoscillator cells, the proportion of neurons responding was notably more sparse (n = 65/286; 23%; data not shown).

In voltage-clamp mode, at a holding potential of −60 mV, the application of TRH (1 μM) to TIDA neurons induced a mean inward current of –18.0 ± 2.3 pA, which was reversible upon washout (n = 5; $p < 0.01$; Figure 6Ba). Ramping holding potential from −120 to +20 mV in the presence (1 μM) and absence of TRH demonstrated that the TRH-induced current reversed at −13.4 mV (n = 4; Figures 6Bb and 6Bc).

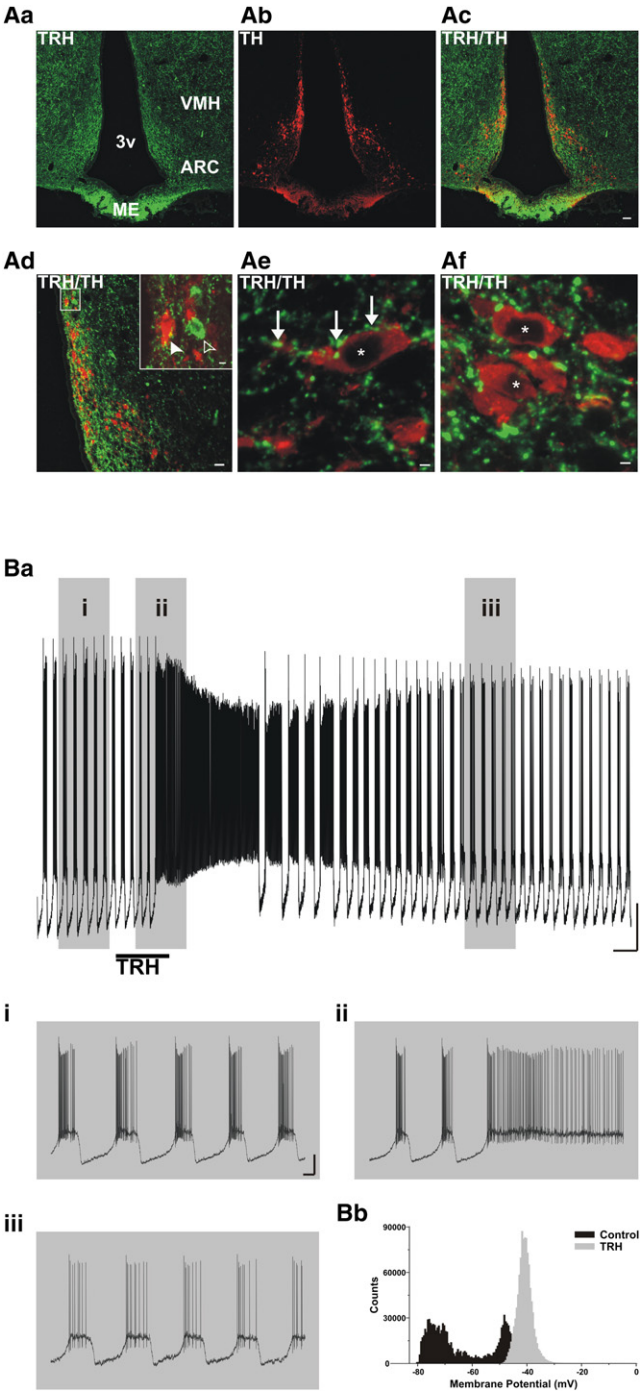

Figure 5. TIDA Neurons Are Densely Innervated by TRH and Respond to TRH Application by Switching from Phasic to Tonic Firing

(Aa–Af) Confocal micrographs from coronal sections of the rat hypothalamus double labeled by immunofluorescence for TRH (green; Aa) and TH (red; Ab). Merged images are shown in (Ac)–(Af). Tyrosine hydroxylase-immunoreactive (-ir) cell bodies are enmeshed in a dense network of TRH-ir terminals (Aa and Ac–Af). Occasional TRH-ir cell bodies are observed that do not stain positive for TH (inset in Ad). High-resolution (Ae and Af) shows TRH-ir terminals forming close appositions (arrows) on somata (asterisk) and proximal dendrites of solitary TH-ir neurons (Ae), and clusters of TH-ir cells surrounded by TRH-ir terminals (Af).

(Ba) Current-clamp recording from an oscillating TIDA neuron. Under control conditions (i), the cell displays stereotypical oscillation. Following application of TRH (1 μM), the cell depolarizes and undergoes a transition from phasic to tonic firing (ii). The oscillation returns after wash of TRH from the recording solution (iii). (Bb) Frequency distribution plot illustrating the shift from bi- to monophasic distribution induced by TRH.

Scale bar indicates 100 μm in (Aa)–(Ac), 50 μm in (Ad) and in inset, 10 μm, 5μm in (Ae) and (Af), 20 mV and 60 s in (Ba), 20 mV and 5 s for (Bai)–(Biii). Arc, arcuate nucleus; ME, median eminence; 3v, third ventricle; VMH, ventromedial hypothalamic nucleus. See also Figure S1.

TRH Modulates Synaptic Transmission in TIDA Cells

Next, we investigated if the TRH-induced excitation of TIDA neurons, in addition to the direct membrane depolarization described above, also involved modulation of synaptic transmission. Changes in the mean frequency and amplitude of synaptic events were analyzed by t test and changes in pooled cumulative frequency distributions by Kolmogorov-Smirnov (KS-2) analysis. Excitatory transmission was investigated at a holding potential of −60 mV and in the presence of BMI to abolish ionotropic GABAergic transmission. Under these conditions, application of TRH (1 μM) induced a marked increase in the mean frequency of spontaneous EPSCs (sEPSCs; Figures 7A–7Ca; n = 4; t test $p < 0.001$; KS-2 $p < 0.001$). Mean sEPSC amplitude showed a trend toward increase, but this difference failed to reach statistical significance ($p = 0.07$; Figure 7Cc). The sEPSC amplitude was, however, significantly increased with regard to cumulative frequency distribution (KS-2 $p < 0.001$; Figure 7Cb). Miniature EPSCs (mEPSCs) were investigated in the presence of TTX with the same holding potential and in bicuculline as above (Figures 7Da and 7Ea). Both frequency (t test $p < 0.001$; KS-2 $p < 0.001$; Figures 7Db and 7Dc) and amplitude (t test $p < 0.01$; KS-2 $p < 0.001$; Figures 7Eb and 7Ec) of mEPSCs were significantly increased following application of TRH (1 μM; n = 5). All changes described above reversed upon washout of TRH. These findings suggest that TRH modulates both presynaptic release and postsynaptic responsiveness of ionotropic glutamatergic transmission in TIDA neurons.

Inhibitory transmission in oscillator neurons was investigated at a holding potential of −60 mV with a "high Cl^-" intracellular recording solution to amplify IPSCs and with CNQX and AP5 added to the extracellular solution to abolish ionotropic glutamatergic transmission (Figure 8A). While the frequency of sIPSCs increased in the presence of TRH (1 μM; Figures 8A–8Ca; n = 7; t test $p < 0.05$; KS-2 $p < 0.001$), the amplitude of spontaneous inhibitory events decreased (Figures 8Ba and 8Ca–8Cc; t test $p < 0.01$; KS-2 $p < 0.001$). The frequency of mIPSCs also increased following application of TRH (1 μM; n = 5; t test $p < 0.001$; KS-2 $p < 0.001$; Figures 8Da–8Ea). Mean mIPSC amplitude change did not reach significance (Figure 8Ec; t test n = 0.12), but the shift in cumulative frequency was statistically significant (Figure 8Eb; KS-2 $p < 0.001$). Taken together, these results indicate that while the dominant effect of TRH on synaptic transmission in TIDA neurons is a facilitation of excitation, a modest activation of inhibitory input also occurs. To determine the effects of TRH on electrotonically isolated TIDA neurons, we assessed spontaneous synaptic input in the presence of gap junction blockers (CBX, 50 μM; 18βGA, 50 μM). Under these conditions, application of TRH (1 μM) also induced an increase in

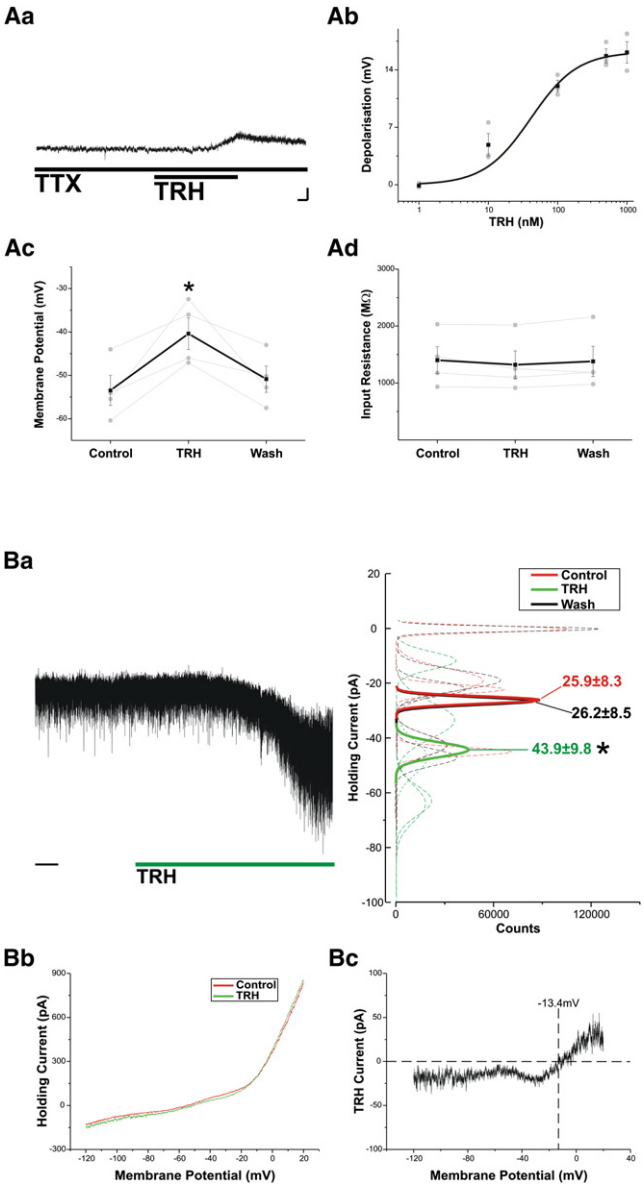

Figure 6. In TIDA Neurons, TRH Activates an Inward Current

(Aa) Current-clamp recording of an oscillator neuron demonstrates that the depolarizing response to TRH (1 μM) endures in the presence of TTX. (Ab) Dose response curve highlighting the relationship between [TRH] and resultant membrane depolarization. All cells (n = 4) were tested with all concentrations sequentially and were recorded in the presence of TTX. Gray dots represent raw values, black the mean, and line is the Hill fit of the mean (n = 3). (Ac) TRH (1 μM) causes a significant change in resting membrane potential (recorded in presence of TTX; n = 4; *p < 0.05). (Ad) No significant change in input resistance is observed (n = 4).

(Ba) Voltage-clamp recording of an oscillator neuron in the presence of TTX. Application of TRH (1 μM) results in an inward current. To the right, Gaussian fits of averaged (solid lines) holding current frequency distributions in control (red), TRH (green), and after wash (black). Raw data used to produce averages shown as dashed lines (n = 5; *p < 0.05). The y axis scale is the same as for raw trace on left. (Bb) Averaged voltage-clamp ramps (n = 4) recorded under control conditions (red) and at the peak of the TRH response (green). (Bc) TRH-induced current subtracted from traces shown in (Bb). Note reversal at −13.4 mV.

the mean frequency of sEPSCs (Figures S2Aa and S2Ab; n = 3) that was significant in KS-2 (Figure S2Aa; $p < 0.001$), although it did not reach significance in the t test (Figure S2Ab; $p = 0.08$). Similarly, sEPSC amplitude in gap junction blockade increased after TRH application (Figures S2Ba and S2Bb; KS-2, $p < 0.001$; t test 0.051). Spontaneous inhibitory input under gap junction blockade was also assessed (n = 4). Similar to conditions of intact electrotonic coupling, sIPSC frequency increased in response to TRH application (Figures S2Ca and S2Cb; KS-2, $p < 0.001$; t test $p < 0.05$), while sIPSC amplitude decreased (Figures S2Da and S2Db; KS-2, $p < 0.001$; t test $p < 0.05$).

DISCUSSION

Although the concept of parvocellular neuroendocrine control of anterior pituitary hormone release was first proposed 60 years ago (Harris, 1948), remarkably little is known about the cellular and network properties of these neurons. We report recordings of identified TIDA neurons and show that these cells exhibit an exceptionally regular and robust oscillation. A subpopulation of rat Arc neurons alternated rhythmically between periods of relative quiescence (DOWN states) and episodes of depolarization crowned by action potential discharge (UP states) with a periodicity of ~20 s. We provide evidence that these oscillator cells are TIDA neurons based on their location in the dorsomedial Arc, their consistent TH-immunoreactivity, and their uptake of the blood-brain barrier impermeable dye Evans Blue. Rhythmic oscillations have previously been reported in Arc cells that contain prepro-neuropeptide Y (NPY) mRNA as detected by PCR (van den Top et al., 2004). Tyrosine hydroxylase and NPY are found in functionally separate neurons (neuroendocrine and ascending, respectively) in the Arc (Everitt et al., 1986). It cannot be excluded that there are separate oscillating populations in this heterogeneous nucleus. We failed, however, to locate oscillating cells that did not stain positive for TH in our sampling. Furthermore, in our investigation, all oscillator cells from Evans Blue-injected animals displayed fluorescence, while Arc NPY cells do not appear to project to the pituitary (Vanhatalo and Soinila, 1996).

The TIDA oscillation was highly synchronized between neurons. The disappearance of rhythmic activity in the presence of CBX and 18βGA, coupled with its persistence under conditions of fast synaptic blockade, suggest that the oscillation is an emergent network property dependent on electrotonic communication. The importance of gap junctions for network rhythms has been established in several brain regions, but has received relatively little attention in the hypothalamus (see Connors and Long, 2004). The phasic firing in neuroendocrine TIDA cells shown here bear similarity to inferior olivary neurons, where electrotonic coupling throughout the network provides a means of synchronizing spiking input to the cerebellar cortex (Llinás and Yarom, 1986). Our data further suggest, however, that although chemical synapses are not necessary for rhythmic activity in

Scale bar in (Aa) 10 mV and 10 s, in (Ba) indicates 20 s. Error bars represent the mean ± SEM.

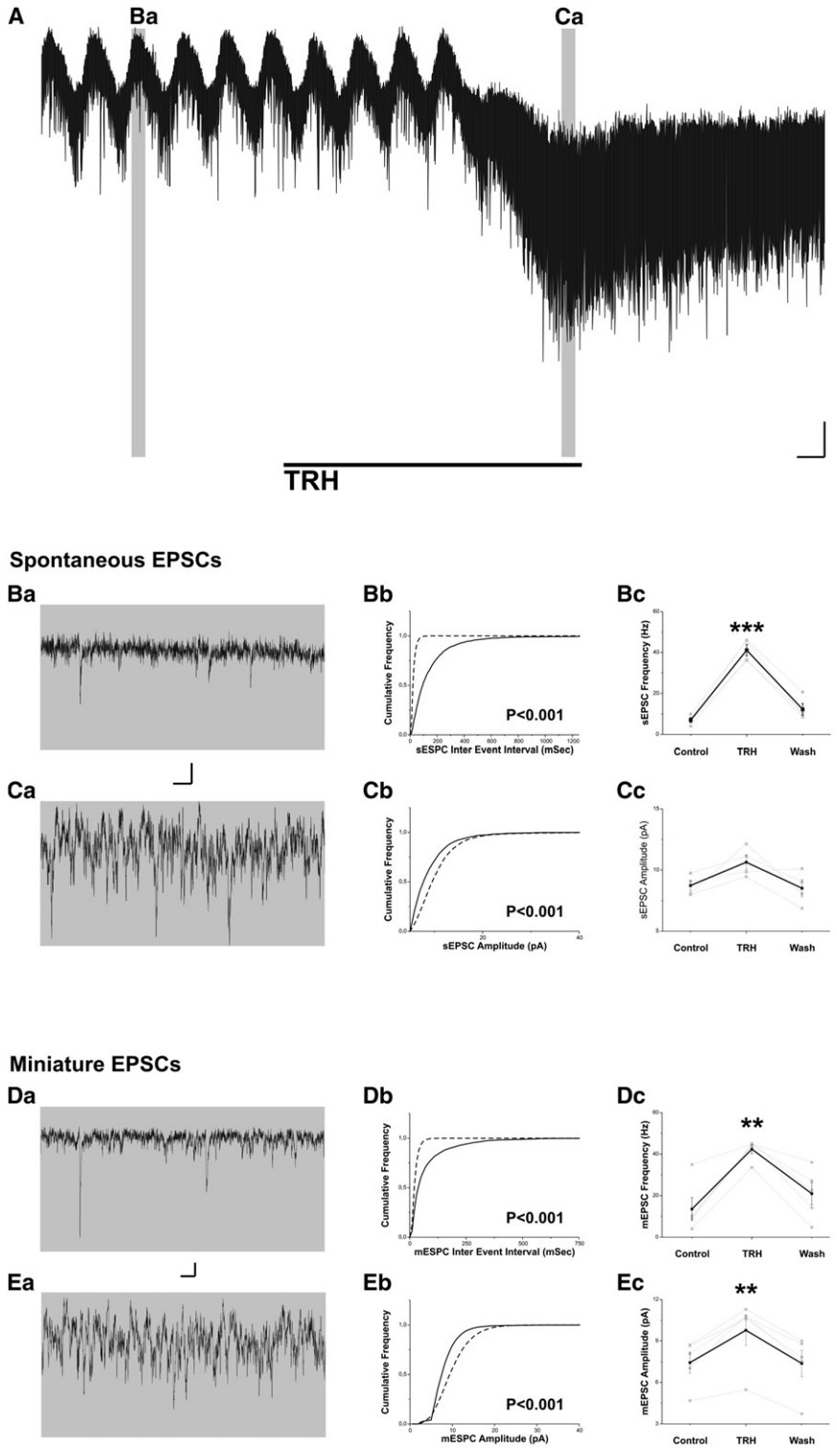

Figure 7. Excitatory Synaptic Transmission in TIDA Neurons Is Facilitated by TRH

(A) Voltage-clamp recording of an oscillator neuron recorded in the presence of BMI to isolate sEPSCs. Expanded traces shown in (Ba) and (Ca) illustrate sEPSCs before and during application of TRH (1 μM), respectively. Sample traces in (Da) and (Ea) illustrate mEPSCs (recorded in the presence of BMI and TTX) before and during application of TRH (1 μM), respectively. TRH increased the amplitude and frequency of both sEPSCs (n = 4) and mEPSCs (n = 5). Pooled cumulative frequency distribution plots for interevent interval are shown in (Bb) and (Db), and for amplitude in (Cb) and (Eb) (full line, control; dashed line, TRH). Changes in mean frequency shown in histograms in (Bc) (n = 4; ***p < 0.001) and (Dc) (n = 5; **p < 0.01); changes in mean amplitude shown in histograms in (Cc) and (Ec). Scale bar in (A) indicates 20 pA and 10 s, in (Ba) and (Ca) 10 pA and 0.05 s, and in (Da) and (Ea) 5 pA and 0.05 s. See also Figure S2. Error bars represent the mean ± SEM.

TIDA neurons, the cells receive substantial postsynaptic input with a significant increase in IPSCs during the UP state. Given the tight coupling between TIDA cells (present data), their GABAergic nature (Everitt et al., 1984), and GABAergic synaptic innervation (van den Pol, 1986), it appears likely that these barrages of inhibition reflect synaptic interconnectivity within the network. The anatomical organization of TIDA neurons we observed, with close clustering of cells and the wide reach of the dendritic tree that they extend within the population, could favor both forms of cell-cell contact and synchronization.

Unlike other hypothalamic-pituitary systems, a unique releasing factor for the lactotrophic axis has to date not been identified (see Samson et al., 2003). Perhaps the best candidate is TRH, since i.v. administration of this peptide results in a prominent surge in plasma prolactin (Bowers et al., 1971; Jacobs et al., 1971). Based on, for example, the presence of TRH receptors on a subpopulation of prolactin-secreting pituicytes (Konaka et al., 1997) and the fact that TRH can cause prolactin secretion from cultured lactotrophs (Smith and Convey, 1975), it has been assumed that this effect takes place at the pituitary level in concert with TRH-stimulated release of thyroid-stimulating hormone (TSH). This conclusion is, however, complicated by the fact that plasma TSH and prolactin secretion do not consistently correlate (e.g., Gautvik et al., 1973). An additional possibility is that TRH modulates TIDA cell discharge at the hypothalamic level. This possibility has not yet been evaluated. Systemic TRH, likely due to the small tri-peptide structure of the peptide, is able to elicit central actions without modulation of the peripheral thyroid axis (Nemeroff et al., 1975; Nishino

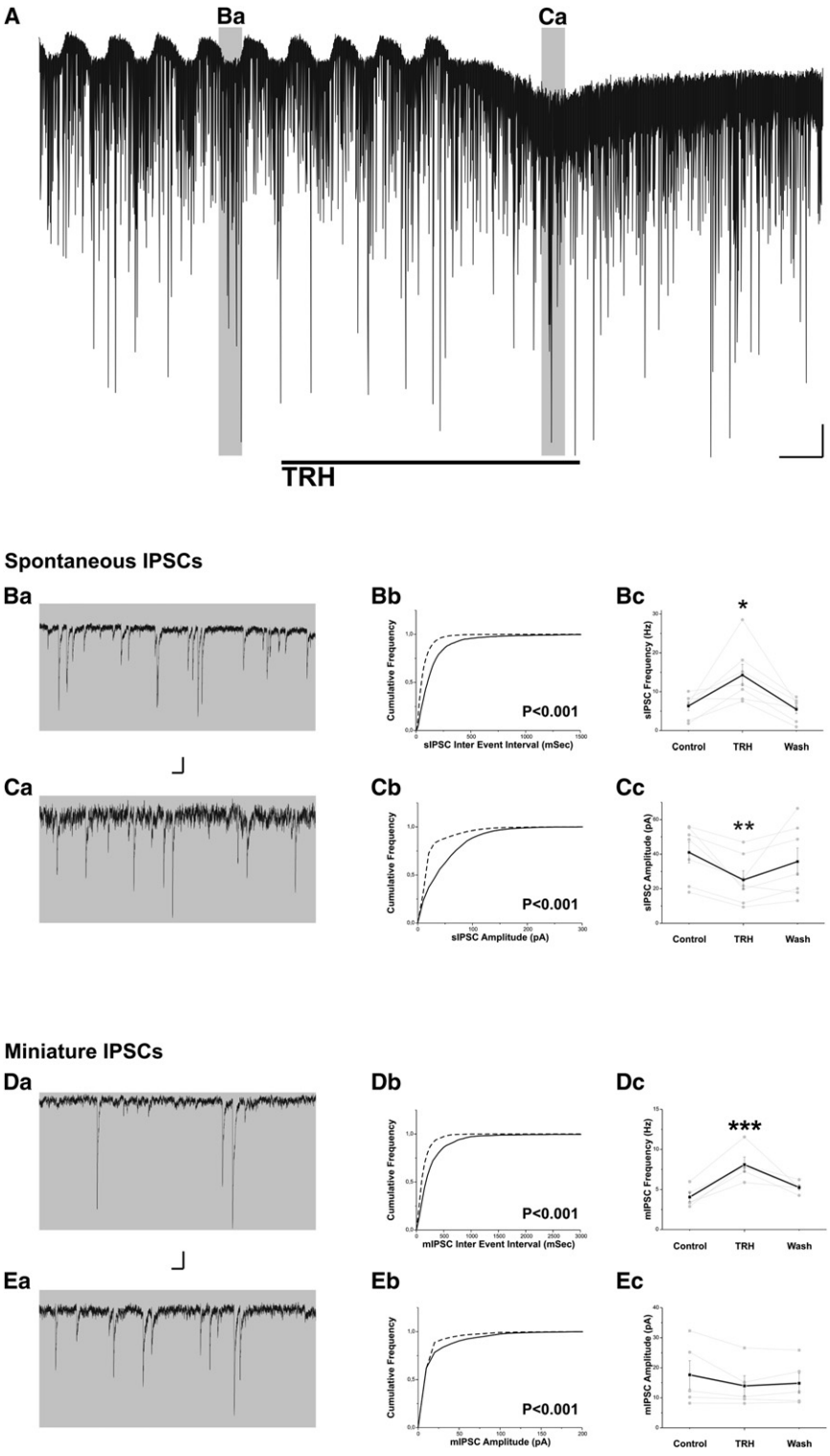

Figure 8. Inhibitory Synaptic Transmission in TIDA Neurons Is Modulated by TRH

(A) Voltage-clamp recording of an oscillator neuron recorded in the presence of CNQX/AP5 to isolate sIPSCs. Expanded traces shown in (Ba) and (Ca) illustrate sIPSCs before and during application of TRH (1 μM), respectively. Sample traces in (Da) and (Ea) illustrate mIPSCs (recorded in the presence of CNQX/AP5 and TTX) before and during application of TRH (1 μM), respectively. TRH decreased the amplitude and increased frequency of both sIPSCs (n = 7) and mIPSCs (n = 5). Pooled cumulative frequency distribution plots for interevent interval are shown in (Bb) and (Db), and for amplitude in (Cb) and (Eb) (full line, control; dashed, TRH). Changes in mean frequency shown in histograms in (Bc) (n = 7; *$p < 0.05$) and (Dc) (n =5; ***$p < 0.001$); changes in mean amplitude shown in histograms in (Cc) (n = 7; **$p < 0.01$) and (Ec). Scale bar in (A) indicates 20 pA and 20 s, in (Ba), (Ca), (Da), and (Ea) 20 pA and 0.2 s. See also Figure S2. Error bars represent the mean ± SEM.

et al., 1997). The prolactin-releasing effect of exogenous TRH could thus well be mediated via hypothalamic interactions, in particular within the Arc where blood-brain barrier permeability is high (Broadwell and Brightman, 1976). The dense innervation of TIDA cells by TRH terminals (present results), strong expression of the TRH-R1 receptor in the dorsal Arc (Heuer et al., 2000; Ebling et al., 2008), and presence of TRH radioligand binding in this nucleus (Manaker et al., 1985) suggest that relevant signaling molecules are available for a direct TRH-TIDA interaction. We demonstrate here a robust, reversible, and dose-dependent depolarization of all immunochemically identified TIDA neurons in response to TRH application.

The TRH-mediated excitation of TIDA neurons involves both post- and presynaptic effects. Postsynaptic effects include a direct membrane depolarization via an inward current that reverses at ~−13 mV. These data suggest that TRH enhances a mixed cation conductance as has been shown in spinal, thalamic, and lateral hypothalamic neurons (Nicoll, 1977; Broberger and McCormick, 2005; Gonzalez et al., 2009). The increased amplitude of mEPSCs in the presence of TRH also indicates an increased responsiveness to glutamatergic inputs in TIDA cells. Conversely, the decreased mIPSC amplitude indicates that the postsynaptic responsiveness to GABAergic inputs was reduced or a reduction in the number of quanta released per event. Presynaptically, application of TRH resulted in a large increase in the frequency of sEPSCs, which contributed to the overall excitation. We also observed a smaller, but significant, increase in sIPSC frequency. This increased frequency of inhibition within the envelope of dominant excitation

is not surprising given the GABAergic nature of TIDA cells (Everitt et al., 1984) and could further reflect TIDA interconnectivity. The source of TRH innervation of the dorsal Arc is not known at present. We observed a few TRH-ir somata adjacent to the TIDA neurons, but it appears unlikely that these scattered cells could contribute such a dense terminal plexus. It remains to be determined if this innervation is supplied by other hypothalamic TRH populations in the paraventricular, dorsomedial, or lateral hypothalamic nuclei (Heuer et al., 2000) or originate elsewhere in the brain.

What could be the functional relevance of the TIDA oscillation described here? We propose that coordination of bursting within this small network serves to increase the population output of hormone into the portal vessels to ensure large accumulations of DA at the lactotroph. Beyond the neuroendocrine innervation of the median eminence, TIDA cells extend only very sparse projections to other brain nuclei (Scott et al., 2003; Dufourny et al., 2005), suggesting that the primary functional implications for the phasic firing is related to its regulation of lactation. Several factors may contribute to making intermittent bursting a more efficient way of transmitting DA inhibition of prolactin release. Intriguingly, low concentrations of DA paradoxically stimulate prolactin release both in vitro and in vivo (Denef et al., 1980; Tagawa et al., 1992; Arey et al., 1993; Burris and Freeman, 1993; Porter et al., 1994; Chang et al., 1997). It has been proposed (Tabak et al., 2007) that with low DA release, D2 receptor stimulation is insufficient to activate the inward rectifier K^+ currents that otherwise would prevent action potential discharge in the lactotroph. The residual D2 stimulation occurring at these DA concentrations, however, is still sufficient to activate fast K^+ currents (I_A and I_{BK}), which potentiate the action potential-dependent Ca^{2+} influx that triggers prolactin exocytosis (Burris and Freeman, 1993; Tabak et al., 2007). In our experiments, the prolactin-releasing peptide TRH abolished repetitive bursting in TIDA cells, replacing it with tonic firing. It is established in other DA (midbrain) systems (Gonon, 1988), as well as in other neuroendocrine (magnocellular) neurons (Dutton and Dyball, 1979), that phasic firing results in substantially enhanced transmitter release as compared to tonic discharge. In the midbrain DA systems, the experimental abolishment of phasic firing has drastic behavioral consequences, disrupting certain forms of learning (Zweifel et al., 2009). While we observed a modest attenuation in firing frequency when TIDA cells switched from oscillatory to continuous discharge in the presence of TRH, it can be noted that in the above-mentioned systems a change in mean firing frequency per se is not required to decrease transmitter release (Gonon, 1988; Dutton and Dyball, 1979). Furthermore, it is possible that with prolonged continuous firing and the loss of DOWN states, de novo synthesis of DA fails to match demand for hormone release. Dopamine repletion may be particularly vulnerable in this neurosecretory system, where transmitter reuptake mechanisms, though active (Bossé et al., 1997), are less efficient than in the CNS (Lookingland et al., 1987). Finally, with the abolishment of bursting, synchronization within the TIDA population would disappear, further limiting the potential for achieving large pituitary concentrations of DA. These mechanisms could all contribute to a TRH-induced switch from high DA inhibiting prolactin secretion to stimulation mediated by decreasing DA release.

This proposed mode of action differs from the mechanisms active in the better-studied gonadotropin system, differences that may reflect the opposite roles of these neuroendocrine systems (inhibition versus stimulation). Rhythmic discharge in gonadotropic hypothalamic neurons is critical for agonist action in the pituitary (Knobil, 1980). Replacing endogenous pulsatile secretion of gonadotropin-releasing hormone (GnRH) with continuous administration results in a paradoxical drop in plasma levels of luteinizing and follicle-stimulating hormone (Nakai et al., 1978). This phenomenon is thought to be the result of adaptation within the signaling machinery downstream of the GnRH receptor (McArdle et al., 1996). However, the rhythms in GnRH (bursting once per hour) are substantially slower than the oscillation periodicity of ~20 s that we observe in TIDA cells. It appears unlikely that the 0.05 Hz frequency of TIDA bursting is reproduced at the lactotroph membrane after passage through the portal capillaries. Thus, it seems reasonable to speculate that the functional role of the TIDA oscillation is not to time prolactin surges but to ensure sufficient inhibitory concentrations of DA in the anterior pituitary.

In summary, the present data describe the synchronized ensemble discharge of TIDA neurons, suggesting a novel principle for the control of prolactin secretion where phase-locked rhythmic oscillations drive dopaminergic inhibition of lactation. Furthermore, our results indicate that TRH-mediated stimulation of prolactin release occurs at the hypothalamic, as well as pituitary, level by shifting TIDA oscillations to tonic discharge.

EXPERIMENTAL PROCEDURES

Animals

Male Sprague-Dawley rats (Scanlab, Sollentuna, Sweden), 22–30 days old, were housed with free access to standard rat chow and tap water in a temperature-controlled environment under 12/12 hr light/dark conditions with lights on at 6 A.M. To identify neuroendocrine cells, four rats were injected in the tail vein with 0.1 ml of the dye Evans Blue (3% in sterile 0.9% NaCl). Slices were prepared as below 5–10 days after dye injection. For this study of the prolactin-inhibitory TIDA cells, we used male rats, where inhibition is likely at its most active and to avoid confounding influence from fluctuations in sex hormones, which are potent endogenous modulators of prolactin secretion. All animal experiments had received prior approval by the local ethical board, Stockholms Norra Djurförsöksetiska Nämnd, and were carried out in accordance with the European Communities Council Directive of 24 Nov. 1986 (86/609/EEC).

Whole-Cell Recordings

For electrophysiological experiments, rats were deeply anesthetized with sodium pentobarbital and decapitated. The brain was rapidly dissected out and placed in an ice-cold and oxygenated (95%O_2/5%CO_2) solution containing (in mM) sucrose (214), KCl (2.0), NaH_2PO_4 (1.2), $NaHCO_3$ (26), $MgSO_4$ (1.3), $CaCl_2$ (2.4), D-glucose (10). The meninges were gently removed, and the brain was blocked and glued to a vibratome (Leica, Wetzlar, Germany) where 250–300 μm thick coronal sections of the hypothalamus containing the Arc were cut and immediately transferred to an artificial CSF solution containing (in mM) NaCl (127), KCl (2.0), NaH_2PO_4 (1.2), $NaHCO_3$ (26), $MgCl_2$ (1.3), $CaCl_2$ (2.4), D-glucose (10), in a continuously oxygenated holding chamber at 35°C. Slices were stored under these conditions for a minimum of 1 hr before recording. For whole-cell recordings, slices were transferred to a submerged chamber and placed on an elevated grid that allows perfusion both above and below the slice. An Axioskop 2 FS Plus upright microscope (Carl Zeiss, Jena, Germany) was used for infrared-differential interference contrast visualization of cells. Recordings were performed at room

temperature (22°C), and slices were continuously perfused with oxygenated artificial CSF (as above) unless otherwise described at a rate of ~5 ml/min. All pharmacological compounds were bath applied.

Whole-cell current- and voltage-clamp recordings were performed with 3–6 MΩ pipettes made from borosilicate glass capillaries (World Precision Instruments, Aston, UK) pulled on a P-97 Flaming/Brown micropipette puller (Sutter, Novato, CA). The intracellular recording solution used in experiments, unless otherwise noted, contained (in mM) Kgluconate (140), KCl (10), HEPES (10), EGTA (1), Na_2ATP (2), pH 7.3 (with KOH), with 0.2% neurobiotin added for subsequent morphological reconstruction of recorded cells. For measurement of inhibitory postsynaptic currents, a modified intracellular solution ("high Cl^-") was used containing (in mM) KCl (150), HEPES (10), EGTA (1), Na_2ATP (2), and 0.2% neurobiotin. Blockade of ionotropic glutamatergic transmission was achieved by adding 10 μM of the AMPA/kainic acid antagonist 6-cyano-7-nitroquinoxaline-2,3-dione (CNQX) and 25 μM of the NMDA antagonist DL-2-amino-5-phosphonopentanoic acid (AP5) to the extracellular recording solution. Blockade of ionotropic GABA transmission was achieved by adding 20 μM of the $GABA_A$ receptor antagonist bicuculline methiodide (BMI) to the extracellular recording solution. The concentration used for tetrodotoxin (TTX) was 0.5 μM. To inhibit Ca^{2+}-dependent synaptic transmission, the extracellular recording solution was modified to contain (in mM) NaCl (127), KCl (2.0), NaH_2PO_4 (1.2), $NaHCO_3$ (26), $MgSO_4$ (9.0), $CaCl_2$ (0.3), D-glucose (10); "low Ca^{2+}/high Mg^{2+}" solution. Recordings were performed using a Multiclamp 700B amplifier (Molecular Devices, Sunnyvale, CA) and pClamp9 software. Slow and fast capacitative components were automatically compensated for. Access resistance was monitored throughout the experiments, and only those cells with stable access resistance (changes <15%) were used for analysis. Liquid junction potential was not compensated. The recorded current was filtered at 2k Hz and sampled at 10k Hz.

Statistical Analysis and Reagents

Data analysis was performed with Originpro8 (OriginLab, Northampton, MA) and Clampfit (Molecular Devices). Results were analyzed using the paired two-tailed Student's t test unless otherwise stated. To determine the TRH-induced current in the presence of TTX, all points histograms were plotted for 20 s of control, TRH, and wash traces, with Gaussian fits performed on the individual and pooled distributions. The mean difference between the Gaussian peaks for control and TRH was used as the value for TRH-induced current. Postsynaptic currents were analyzed using Mini Analysis 6.0.9 (Synaptosoft, Decatur, GA). Detection threshold was set at 3-fold the root-mean-square (RMS) noise level, which typically was 3–6 pA. Frequency, interevent-interval, and amplitudes were calculated as a mean of the values obtained during a 50 s recording period. The two-sample Kolmogorov-Smirnov (K-S2) test was used to compare pooled cumulative frequency distributions of each component in the absence versus the presence of TRH. The critical value for statistical significance was set at $p < 0.05$, unless indicated otherwise. Data are presented as means ± SEM unless otherwise stated. Thyrotropin-releasing hormone was purchased from Phoenix Pharmaceuticals (Burlingame, CA), neurobiotin was purchased from Vector Labs (Burlingame, CA), tetrodotoxin was purchased from Alomone Labs (Jerusalem, Israel), and CNQX, AP5, BMI, CBX, 18βGA, and Evans Blue were from Sigma (St Louis, MO).

Immunofluorescence

To optimize detection of cell bodies, rats (n = 3) were injected unilaterally i.c.v. with colchicine prior to perfusion. Twenty-four hours later, the animals were anesthetized with an i.p. overdose of sodium pentobarbital and perfused via the ascending aorta with 50 ml of Tyrode's Ca^{2+}-free solution (37°C) followed by 50 ml fixative solution containing 4% paraformaldehyde, 0.5% glutaraldehyde, and 0.2% picric acid in 0.16 M phosphate buffer, pH 6.9 (37°C), followed by 300 ml of the same but ice-cold fixative. The brains were dissected out, immersed in the same fixative for 90 min, and rinsed for 20 hr in 0.1 M phosphate buffer (pH 7.4) containing 10% sucrose. Brains were then cut in 1 mm slabs and rinsed in phosphate buffer, incubated for 30 min in 0.1% sodium borohydride, rinsed repeatedly in phosphate buffer, and stored in 10% sucrose solution. Brain slabs were reassembled in appropriate order, frozen, sectioned in the coronal plane at 14 μm thickness on a cryostat (Microm, Heidelberg, Germany), and thaw-mounted onto gelatin-coated glass slides.

Immunofluorescence was performed as previously described (Broberger et al., 1999). Briefly, hypothalamic sections containing the arcuate nucleus were incubated with a cocktail of polyclonal rabbit anti-TRH antiserum (1:8000; generous gift of Dr. T. Visser; see Klootwijk et al., 1995) and monoclonal mouse anti-tyrosine hydroxylase antibodies (1:2000; Millipore, Billerica, MA) in 0.3% Triton X-100/0.01 M PBS, at 4°C for 16 hr. The tissue was then first processed using the tyramide signal amplification (TSA) procedure (Perkin-Elmer, Waltham, MA) for detection of TRH staining. Sections were rinsed in TNT buffer (0.1 M Tris, 0.15 M NaCl, and 0.05% Tween 20), preincubated with TNB blocking reagent (as supplied with the TSA kit; Perkin Elmer) for 30 min, and incubated for another 30 min with horseradish-peroxidase-conjugated swine anti-rabbit immunoglobulin (1:200 in TNB buffer; Dako, Glostrup, Denmark). The sections were then rinsed and incubated for 10 min with tyramide-conjugated fluorescein (1:100 in amplification diluent as supplied with the TSA kit; Perkin Elmer). For detection of TH staining, the sections were subsequently rinsed in 0.01 M PBS, incubated with Cy-3-conjugated secondary antiserum (1:200; Jackson ImmunoResearch, Newmarket, UK), diluted in 0.3% Triton X-100/0.01M PBS for 30 min at 37°C, and subsequently mounted with glycerol supplemented with anti-fade agent (2.5% 1,4-diazabicyclo[2.2.2]octane).

Reconstruction and Staining of Recorded Cells

Immediately after recording, slices were immersion-fixed in 4% paraformaldehyde/0.2% picric acid for 16 hr at 4°C, and rinsed for a minimum 6 hr in 0.1 M phosphate buffer (pH 7.4) containing 0.2% bacitracin and 0.1% sodium azide. Slices were then incubated free floating with fluorescein isothiocyanate-conjugated avidin (Invitrogen, Carlsbad, CA) diluted 1:3000 in 0.6% Triton X-100/0.01 M PBS for 48 hr at 4°C. Following 6 hr of rinsing in PBS, slices were incubated for 72 hr in monoclonal anti-TH antibodies (as above) diluted 1:2000 in 0.6% Triton X-100/0.01 M PBS, rinsed for 6 hr in PBS, incubated for 16 hr in Cy-3-conjugated donkey-anti-mouse IgG antiserum (Jackson ImmunoResearch) diluted 1:400 in 0.6% Triton X-100/0.01 M PBS, rinsed for an additional 6 hr in PBS, and mounted and coverslipped on glass slides with glycerol and anti-fade agent as above. Stained sections and slices were analyzed in a Carl Zeiss LSM 510 META confocal scanning laser microscope, and micrographs were obtained using Start LSM Image Browser software. For final images, only brightness and contrast were adjusted digitally.

SUPPLEMENTAL INFORMATION

Supplemental Information includes two supplemental figures and can be found with this article online at doi:10.1016/j.neuron.2009.12.024.

ACKNOWLEDGMENTS

Antiserum against TRH was generously provided by Dr. T. Visser. The authors thank Kylie Foo for help with figures. This study was supported by the Wenner-Gren Foundations, Knut och Alice Wallenberg's Foundation (KAW 2004.0150), the Rut and Arvid Wolff Foundation, the Novo-Nordisk Foundation, the Magnus Bergvall Foundation, Swedish Research Council, the Åke Wiberg Foundation, the Royal Swedish Academy of Sciences, Längmanska Kulturfonden, Petrus and Augusta Hedlund's Foundation, the Axel Linder Foundation, the Golje Foundation, the Lars Hierta Memorial Foundation, the Hagberg Foundation, the Jeansson Foundations, the O.E. and Edla Johansson Foundation, the Fredrik and Ingrid Thuring Foundation, and the European Commission Coordination Action ENINET (contract number LSHM-CT-2005-19063). D.J.L. is supported by a postdoctoral fellowship from the Wenner-Gren Foundations.

Accepted: December 18, 2009
Published: January 27, 2010

REFERENCES

Arey, B.J., Burris, T.P., Basco, P., and Freeman, M.E. (1993). Infusion of dopamine at low concentrations stimulates the release of prolactin from alpha-methyl-p-tyrosine-treated rats. Proc. Soc. Exp. Biol. Med. *203*, 60–63.

Ben-Jonathan, N., and Hnasko, R. (2001). Dopamine as a prolactin (PRL) inhibitor. Endocr. Rev. *22*, 724–763.

Björklund, A., Moore, R.Y., Nobin, A., and Stenevi, U. (1973). The organization of tubero-hypophyseal and reticulo-infundibular catecholamine neuron systems in the rat brain. Brain Res. *51*, 171–191.

Bossé, R., Fumagalli, F., Jaber, M., Giros, B., Gainetdinov, R.R., Wetsel, W.C., Missale, C., and Caron, M.G. (1997). Anterior pituitary hypoplasia and dwarfism in mice lacking the dopamine transporter. Neuron *19*, 127–138.

Bowers, C.Y., Friesen, H.G., Hwang, P., Guyda, H.J., and Folkers, K. (1971). Prolactin and thyrotropin release in man by synthetic pyroglutamyl-histidyl-prolinamide. Biochem. Biophys. Res. Commun. *45*, 1033–1041.

Broadwell, R.D., and Brightman, M.W. (1976). Entry of peroxidase into neurons of the central and peripheral nervous systems from extracerebral and cerebral blood. J. Comp. Neurol. *166*, 257–283.

Broberger, C., and McCormick, D.A. (2005). Excitatory effects of thyrotropin-releasing hormone in the thalamus. J. Neurosci. *25*, 1664–1673.

Broberger, C., Visser, T.J., Kuhar, M.J., and Hökfelt, T. (1999). Neuropeptide Y innervation and neuropeptide-Y-Y1-receptor-expressing neurons in the paraventricular hypothalamic nucleus of the mouse. Neuroendocrinology *70*, 295–305.

Burris, T.P., and Freeman, M.E. (1993). Low concentrations of dopamine increase cytosolic calcium in lactotrophs. Endocrinology *133*, 63–68.

Burrow, G.N., Wortzman, G., Rewcastle, N.B., Holgate, R.C., and Kovacs, K. (1981). Microadenomas of the pituitary and abnormal sellar tomograms in an unselected autopsy series. N. Engl. J. Med. *304*, 156–158.

Chan-Palay, V., Záborszky, L., Köhler, C., Goldstein, M., and Palay, S.L. (1984). Distribution of tyrosine-hydroxylase-immunoreactive neurons in the hypothalamus of rats. J. Comp. Neurol. *227*, 467–496.

Chang, A., Shin, S.H., and Pang, S.C. (1997). Dopamine D2 receptor mediates both inhibitory and stimulatory actions on prolactin release. Endocrine *7*, 177–182.

Chorev, E., Yarom, Y., and Lampl, I. (2007). Rhythmic episodes of subthreshold membrane potential oscillations in the rat inferior olive nuclei in vivo. J. Neurosci. *27*, 5043–5052.

Clemens, J.A., Smalstig, E.B., and Sawyer, B.D. (1974). Antipsychotic drugs stimulate prolactin release. Psychopharmacology (Berl.) *40*, 123–127.

Connor, J.A., and Stevens, C.F. (1971). Voltage clamp studies of a transient outward membrane current in gastropod neural somata. J. Physiol. *213*, 21–30.

Connors, B.W., and Long, M.A. (2004). Electrical synapses in the mammalian brain. Annu. Rev. Neurosci. *27*, 393–418.

Davidson, J.S., Baumgarten, I.M., and Harley, E.H. (1986). Reversible inhibition of intercellular junctional communication by glycyrrhetinic acid. Biochem. Biophys. Res. Commun. *134*, 29–36.

Denef, C., Manet, D., and Dewals, R. (1980). Dopaminergic stimulation of prolactin release. Nature *285*, 243–246.

Dufourny, L., Caraty, A., Clarke, I.J., Robinson, J.E., and Skinner, D.C. (2005). Progesterone-receptive dopaminergic and neuropeptide Y neurons project from the arcuate nucleus to gonadotropin-releasing hormone-rich regions of the ovine preoptic area. Neuroendocrinology *82*, 21–31.

Dutton, A., and Dyball, R.E. (1979). Phasic firing enhances vasopressin release from the rat neurohypophysis. J. Physiol. *290*, 433–440.

Ebling, F.J., Wilson, D., Wood, J., Hughes, D., Mercer, J.G., Morgan, P.J., and Barrett, P. (2008). The thyrotropin-releasing hormone secretory system in the hypothalamus of the Siberian hamster in long and short photoperiods. J. Neuroendocrinol. *20*, 576–586.

Everitt, B.J., Hökfelt, T., Wu, J.Y., and Goldstein, M. (1984). Coexistence of tyrosine hydroxylase-like and gamma-aminobutyric acid-like immunoreactivities in neurons of the arcuate nucleus. Neuroendocrinology *39*, 189–191.

Everitt, B.J., Meister, B., Hökfelt, T., Melander, T., Terenius, L., Rökaeus, A., Theodorsson-Norheim, E., Dockray, G., Edwardson, J., Cuello, C., et al. (1986). The hypothalamic arcuate nucleus-median eminence complex: immunohistochemistry of transmitters, peptides and DARPP-32 with special reference to coexistence in dopamine neurons. Brain Res. *396*, 97–155.

Freeman, M.E., Kanyicska, B., Lerant, A., and Nagy, G. (2000). Prolactin: structure, function, and regulation of secretion. Physiol. Rev. *80*, 1523–1631.

Fuxe, K. (1964). Cellular localization of monoamines in the median eminence and the infundibular stem of some mammals. Z. Zellforsch. Mikrosk. Anat. *61*, 710–724.

Gautvik, K.M., Weintraub, B.D., Graeber, C.T., Maloof, F., Zuckerman, J.E., and Tashjian, A.H., Jr. (1973). Serum prolactin and TSH: effects of nursing and pyroGlu-His-ProNH2 administration in postpartum women. J. Clin. Endocrinol. Metab. *37*, 135–139.

Gonon, F.G. (1988). Nonlinear relationship between impulse flow and dopamine released by rat midbrain dopaminergic neurons as studied by in vivo electrochemistry. Neuroscience *24*, 19–28.

Gonzalez, A., Horjales-Araujo, E., Fugger, L., Broberger, C., and Burdakov, D. (2009). Stimulation of orexin/hypocretin neurones by thyrotropin-releasing hormone. J. Physiol. *587*, 1179–1186.

Harris, G.W. (1948). Neural control of the pituitary gland. Physiol. Rev. *28*, 139–179.

Hatton, G.I., Ho, Y.W., and Mason, W.T. (1983). Synaptic activation of phasic bursting in rat supraoptic nucleus neurones recorded in hypothalamic slices. J. Physiol. *345*, 297–317.

Heuer, H., Schäfer, M.K., O'Donnell, D., Walker, P., and Bauer, K. (2000). Expression of thyrotropin-releasing hormone receptor 2 (TRH-R2) in the central nervous system of rats. J. Comp. Neurol. *428*, 319–336.

Hökfelt, T. (1967). The possible ultrastructural identification of tubero-infundibular dopamine containing nerve endings in the median eminence of the rat. Brain Res. *5*, 121–123.

Jacobs, L.S., Snyder, P.J., Wilber, J.F., Utiger, R.D., and Daughaday, W.H. (1971). Increased serum prolactin after administration of synthetic thyrotropin releasing hormone (TRH) in man. J. Clin. Endocrinol. Metab. *33*, 996–998.

Katz, B. (1949). Les constantes électriques de la membrane de muscle. Arch. Sci. Physiol. (Paris) *2*, 285–299.

Klootwijk, W., Vaessen, L.M., Bernard, B.F., Rondeel, J.M., De Greef, W.J., and Visser, T.J. (1995). Production and characterization of monoclonal and polyclonal antibodies against thyrotropin-releasing hormone. Hybridoma *14*, 285–290.

Knobil, E. (1980). The neuroendocrine control of the menstrual cycle. Recent Prog. Horm. Res. *36*, 53–88.

Konaka, S., Yamada, M., Satoh, T., Ozawa, H., Watanabe, E., Takata, K., and Mori, M. (1997). Expression of thyrotropin-releasing hormone (TRH) receptor mRNA in somatotrophs in the rat anterior pituitary. Endocrinology *138*, 827–830.

Llinás, R., and Yarom, Y. (1986). Oscillatory properties of guinea-pig inferior olivary neurones and their pharmacological modulation: an in vitro study. J. Physiol. *376*, 163–182.

Lookingland, K.J., Jarry, H.D., and Moore, K.E. (1987). The metabolism of dopamine in the median eminence reflects the activity of tuberoinfundibular neurons. Brain Res. *419*, 303–310.

Lüthi, A., and McCormick, D.A. (1998). H-current: properties of a neuronal and network pacemaker. Neuron *21*, 9–12.

Manaker, S., Winokur, A., Rostene, W.H., and Rainbow, T.C. (1985). Autoradiographic localization of thyrotropin-releasing hormone receptors in the rat central nervous system. J. Neurosci. *5*, 167–174.

McArdle, C.A., Willars, G.B., Fowkes, R.C., Nahorski, S.R., Davidson, J.S., and Forrest-Owen, W. (1996). Desensitization of gonadotropin-releasing hormone action in alphaT3-1 cells due to uncoupling of inositol 1,4,5-trisphosphate generation and Ca2+ mobilization. J. Biol. Chem. *271*, 23711–23717.

Meltzer, H.Y., and Fang, V.S. (1976). The effect of neuroleptics on serum prolactin in schizophrenic patients. Arch. Gen. Psychiatry *33*, 279–286.

Nakai, Y., Plant, T.M., Hess, D.L., Keogh, E.J., and Knobil, E. (1978). On the sites of the negative and positive feedback actions of estradiol in the control

of gonadotropin secretion in the rhesus monkey. Endocrinology *102*, 1008–1014.

Nemeroff, C.B., Prange, A.J., Jr., Bissette, G., Breese, G.R., and Lipton, M.A. (1975). Thyrotropin-releasing hormone (TRH) and its beta-alanine analogue: potentiation of the anticonvulsant potency of phenobarbital in mice. Psychopharmacol. Commun. *1*, 305–317.

Nicoll, R.A. (1977). Excitatory action of TRH on spinal motoneurones. Nature *265*, 242–243.

Nishino, S., Arrigoni, J., Shelton, J., Kanbayashi, T., Dement, W.C., and Mignot, E. (1997). Effects of thyrotropin-releasing hormone and its analogs on daytime sleepiness and cataplexy in canine narcolepsy. J. Neurosci. *17*, 6401–6408.

Porter, T.E., Grandy, D., Bunzow, J., Wiles, C.D., Civelli, O., and Frawley, L.S. (1994). Evidence that stimulatory dopamine receptors may be involved in the regulation of prolactin secretion. Endocrinology *134*, 1263–1268.

Samson, W.K., Taylor, M.M., and Baker, J.R. (2003). Prolactin-releasing peptides. Regul. Pept. *114*, 1–5.

Scott, C.J., Clarke, I.J., and Tilbrook, A.J. (2003). Neuronal inputs from the hypothalamus and brain stem to the medial preoptic area of the ram: neurochemical correlates and comparison to the ewe. Biol. Reprod. *68*, 1119–1133.

Smith, V.G., and Convey, E.M. (1975). TRH-stimulation of prolactin release from bovine pituitary cells. Proc. Soc. Exp. Biol. Med. *149*, 70–74.

Tabak, J., Toporikova, N., Freeman, M.E., and Bertram, R. (2007). Low dose of dopamine may stimulate prolactin secretion by increasing fast potassium currents. J. Comput. Neurosci. *22*, 211–222.

Tagawa, R., Takahara, J., Sato, M., Niimi, M., Murao, K., and Ishida, T. (1992). Stimulatory effects of quinpirole hydrochloride, D2-dopamine receptor agonist, at low concentrations on prolactin release in female rats in vitro. Life Sci. *51*, 727–732.

Tazerart, S., Vinay, L., and Brocard, F. (2008). The persistent sodium current generates pacemaker activities in the central pattern generator for locomotion and regulates the locomotor rhythm. J. Neurosci. *28*, 8577–8589.

van den Pol, A.N. (1986). Tyrosine hydroxylase immunoreactive neurons throughout the hypothalamus receive glutamate decarboxylase immunoreactive synapses: a double pre-embedding immunocytochemical study with particulate silver and HRP. J. Neurosci. *6*, 877–891.

van den Pol, A.N., Herbst, R.S., and Powell, J.F. (1984). Tyrosine hydroxylase-immunoreactive neurons of the hypothalamus: a light and electron microscopic study. Neuroscience *13*, 1117–1156.

van den Top, M., Lee, K., Whyment, A.D., Blanks, A.M., and Spanswick, D. (2004). Orexigen-sensitive NPY/AgRP pacemaker neurons in the hypothalamic arcuate nucleus. Nat. Neurosci. *7*, 493–494.

Vanhatalo, S., and Soinila, S. (1996). Pituitary gland receives both central and peripheral neuropeptide Y innervation. Brain Res. *740*, 253–260.

Wakerley, J.B., and Lincoln, D.W. (1973). The milk-ejection reflex of the rat: a 20- to 40-fold acceleration in the firing of paraventricular neurones during oxytocin release. J. Endocrinol. *57*, 477–493.

Weiss, M.L., and Cobbett, P. (1992). Intravenous injection of Evans Blue labels magnocellular neuroendocrine cells of the rat supraoptic nucleus in situ and after dissociation. Neuroscience *48*, 383–395.

Zweifel, L.S., Parker, J.G., Lobb, C.J., Rainwater, A., Wall, V.Z., Fadok, J.P., Darvas, M., Kim, M.J., Mizumori, S.J., Paladini, C.A., et al. (2009). Disruption of NMDAR-dependent burst firing by dopamine neurons provides selective assessment of phasic dopamine-dependent behavior. Proc. Natl. Acad. Sci. USA *106*, 7281–7288.